Accelerated Electrons in Cassiopeia A: Thermal and Electromagnetic Effects

J. Martin Laming

E. O. Hulburt Center for Space Research, Naval Research Laboratory, Code 7674L, Washington DC 20375

jlaming@ssd5.nrl.navy.mil

ABSTRACT

We consider in more detail a model previously proposed for the hard X-ray (> 10 keV) emission observed from the supernova remnant Cas A, whereby electrons are accelerated by lower-hybrid waves and radiate bremsstrahlung. We consider both cold and thermal plasma limits of the modified two-stream instability that generates the lower-hybrid waves, and by studying time dependent ionization balance for various components of the Cas A ejecta and shocked circumstellar medium, find locations within the shell where one or other of the instabilities may occur. Either instability can be effective, with the cold plasma instability imposing fewer constraints on the shocked reflected ion population responsible for exciting the waves. The instability must be located in the ejecta shocked at the earliest times and therefore closest to the contact discontinuity where magnetic fields are expected to be the strongest. The energy deposited in this ejecta by collisions between accelerated and ambient electrons is broadly consistent with that required to reheat this ejecta to the observed temperature of $\sim 4 \times 10^7$ K.

Subject headings: acceleration of particles—radiation mechanisms: non-thermal—shock waves—supernova remnants

1. Introduction

The supernova remnant Cassiopeia A has long intrigued astonomers across the entire electromagnetic spectrum. Long known as the brightest radio source in the northern sky (Reber 1944; Ryle & Smith 1948), it has also recently been detected in TeV γ rays (Aharonian

et al. 2001), and is most likely the remnant of a putative supernova observed as a 6th magnitude star by Flamsteed in 1680. The discovery of hard X-ray continuum emission extending out to 100 keV has stimulated interest in electron acceleration in its shock waves. As discussed in a recent paper (Laming 2001), the original interpretation of this emission as synchrotron radiation from highly relativistic electrons (Allen et al. 1997) deserves further study. Unlike in the cases of SN 1006 (Koyama et al. 1995), G347.3-0.5 (Slane et al. 1999; Koyama et al. 1997), and now also G266.1-1.2 (Slane et al. 2000), where the X-ray continuum is strong enough to completely mask the line emission that should also be present, the continuum in Cas A is merely a high energy "tail" to the otherwise Maxwellian thermal bremsstrahlung continuum, as shown in Figure 1. (Figure 1 also shows some models discussed in detail below). It is thus possible that such emission could be the result of electrons accelerated by collisionless processes other than first order Fermi acceleration at shock fronts.

Such a scenario is possible because the shock transition occurs on a length scale much shorter than particle mean free paths to Coulomb collisions. Assuming that the gas pressure >> magnetic pressure in the downstream plasma, the temperature T_a reached by particle species a with mass m_a is given by conservation of energy, momentum and particles across the shock discontinuity by

$$k_{\rm B}T_a = \frac{3}{16}m_a v_s^2 \tag{1}$$

for shock velocity v_s . Thus in the limit of true collisionless plasma, the particles will have temperatures proportional to their masses, i.e. protons will have a temperature $m_i/m_e = 1836$ times that of the electrons. Obviously in realistic conditions Coulomb equilibration will take place, with rate (Spitzer 1978, see also Appendix B)

$$\frac{d\Delta T}{dt} = -0.13Z^2 n_e \frac{\Delta T}{AT_e^{3/2}} \tag{2}$$

in c.g.s. units, where $\Delta T = T_i - T_e$, and the ions have charge Z and atomic mass A. However collisionless processes involving the generation of plasma waves at the shock front and the associated electron heating by Landau damping or stochastic processes can operate on a much faster timescale. Recent simulations of such processes are given by Dieckmann et al. (2000) and Shimada & Hoshino (2000) for quasi perpendicular shocks (magnetic field in the plane of the shock front) and by Bykov & Uvarov (1999) for a quasi parallel shock (magnetic field parallel to shock velocity vector), where shock heated electron distributions characterized by Maxwellians at low energies going over into power law distributions at high energies are frequently seen.

Although these results appear qualitatively consistent with the observed X-ray spectra of Cas A, the situation is complicated by the fact that optical (Ghavamian et al. 2001) and UV (Laming et al. 1996) diagnostics for collisionless electron heating at fast shocks

(admittedly in other supernova remnants, Tycho and SN 1006) give essentially no electron heating beyond that implied by the shock jump conditions, equation (1). Similar results have been found in X-ray spectra for E0102.2-7219 (Hughes et al. 2000), SN 1987A (Burrows et al. 2000), and SN 1993J (Fransson, Lundqvist, & Chevalier 1996). Laming (1998, 2000, 2001) speculated that the extrapolation involved from the modest Mach numbers (of order 1-10) of the simulated shocks to the very high (> 100) Mach numbers for forward and reverse shocks in supernova remnants might not be valid. The reasoning behind this is that the higher Mach number shocks become progressively more turbulent (c.f. Tidman & Krall 1971; Tokar et al. 1986; Cargill & Papadopoulos 1988). Although this appears to have no effect on the simulations, these have only one spatial dimension. In two or three dimensions the conjecture is that the shock reflected ions, while still quasi-monoenergetic, no longer behave as a "beam", now having a much larger distribution in pitch angle. The consequence of this is that the preshock instabilities heating the electrons are now no longer reactive in nature but kinetic, and have growth rates low enough that insignificant wave growth and hence electron heating can occur before the preshock plasma is overrun by the shock front itself. Reactive and kinetic instabilities are discussed more fully in Appendix A.1.

For this reason Laming (2001) investigated a slightly different mechanism; the excitation of lower hybrid waves and their consequent acceleration of electrons as a result of secondary shocks passing through the presumed region of strong magnetic field in Cas A. Lower hybrid waves are electrostatic ion oscillations, which can occur in magnetic fields strong enough that the electron gyroradius is smaller than the lower hybrid wavelength. Due to this necessary magnetization of the electrons, the waves propagate preferentially across magnetic field lines. The parallel component of the wavevector $k_{||}/k < \omega_{pi}/\omega_{pe}$. Since $\omega/k_{\perp} \sim (m_e/m_i)^{1/2} \omega/k_{||}$ the wave can simultaneously be in resonance with ions moving across the magnetic field and electrons moving along magnetic field lines, which facilitates collisionless energy exchange between ions and electrons on timescales much faster than that associated with Coulomb collisions. A cold plasma theory for lower-hybrid waves is given in the Appendix of Laming (2001). They have also been previously discussed in connection with cometary X-ray emission, supernova remnant shock waves and Advection Dominated Accretion Flows (ADAFS) (Vaisberg et al. 1983; Krasnosel'skikh et al. 1985; Bingham et al. 1997; Shapiro et al. 1999; Bingham et al. 2000; Begelman & Chiueh 1988), and observed in situ together with accelerated electrons at Halley's comet (Gringauz et al. 1986; Klimov et al. 1986).

Lower hybrid waves are especially attractive to consider due to the strong magnetic fields inferred to exist in Cas A (e.g. Longair 1994), near the contact discontinuity between ambient circumstellar material shocked by the blast wave and supernova ejecta heated by the reverse shock. The situation is shown schematically in Figure 2. The explosion drives a blast wave into the surrounding circumstellar medium. As this begins to sweep up more plasma

behind it and decelerates, a reverse shock develops which moves back into the ejecta (in a Lagrangian sense; it is still expanding in Eulerian coordinates), with a contact discontinuity between the reverse shocked ejecta and forward shocked circumstellar medium. The dense shocked ejecta being decelerated by the much less dense shocked circumstellar medium is subject to a Rayleigh-Taylor instability, which is the likely mechanism for the magnetic field amplification. Also shown in Figure 2 are two of the various classes of knots or clumps of material in Cas A that are particularly conspicuous in optical observations. Quasi-stationary floculli (QSFs) are seen ahead of the forward shock and fast moving knots (FMKs) ahead of the reverse shock. As these shocks run into the density contrasts represented by these structures, they split into a transmitted shock that propagates through the clump and eventually destroys it, and a reflected shock that moves back towards the contact discontinuity. It is these reflected shocks that in our model generate the lower hybrid waves and accelerated electrons in the high magnetic field region.

In this paper we extend the analysis of Laming (2001) to more realistic thermal plasma conditions in Cas A. These are taken from time dependent ionization balance calculations based on analytic expressions for the hydrodynamics from McKee & Truelove (1995), and updated in Truelove & McKee (1999). Section 2 develops the plasma theory for lower hybrid waves in thermal conditions. Section 3 describes the ionization balance calculations with and without the extra collisionless electron heating. Since the mechanism depends on having strong magnetic fields in the shell of Cas A, amplified presumably from seed fields by a Rayleigh-Taylor instability, the history of which over the lifetime of the remnant is presently unknown, it is not possible to calculate definitively the hard X-ray spectrum. However if this model is basically correct, a number of inferences can be made about the nature of the plasma in Cas A, and these are discussed in section 4, followed by conclusions in section 5. Many of the mathematical details in section 2 and 3 are given in the Appendices.

2. Cas A and Lower Hybrid Waves Revisited

In a previous paper (Laming 2001) a theory of the growth of lower-hybrid waves was described in the cold plasma approximation (i.e. where the wave frequency $\omega >> \sqrt{2}kv_i$ and the electron cyclotron frequency $\Omega_e >> k_{\perp}v_e$; v_e and v_i are the electron and ion thermal velocities respectively), where ions reflected from shocks propagating throughout the shell of Cas A generate waves through a modified two stream instability at a perpendicular shock. In this case, waves moving at angle θ to the magnetic field direction given by $\cos \theta = \omega_{pi}/\omega_{pe}$ are preferentially excited, where ω_{pi} and ω_{pe} are the ion and electron plasma frequencies respectively. This is because waves at this angle have a group velocity away from the shock

equal to the shock velocity itself (McClements et al. 1997), and hence stay in contact with the shock reflected ions for arbitrary lengths of time. This allows large wave amplitudes to develop, even though the growth rates may be small. These waves are excited by ions returning to the shock front with velocity $2v_s$ directed along to shock velocity vector. As the shock becomes quasi-parallel this feature disappears, since the wave group velocity is no longer in the same direction as the shock velocity. The generalization of this theory for thermal electrons and ions is given in Appendix A. Where $\omega >> \sqrt{2}kv_i$, it is found that outgoing ions can now excite the necessary waves, propagating at direction cosines essentially the same as those found in the cold plasma limit for the returning ions, i.e. $x^2 \sim \omega_{pi}^2/\omega_{pe}^2$. In the opposite case, $\omega << \sqrt{2}kv_i$, again only returning ions can excite the waves, but for a given wavevector do so at a variety of small direction cosines.

In the hot ion limit ($\omega \ll \sqrt{2kv_i}$) waves can be generated with a range of direction cosines and frequencies, so we now proceed to determine the wave direction cosine and frequency at which the net growth rate is maximized in this limit. The growth rate due to a Maxwellian ion distribution moving with bulk velocity \vec{U} in the limit $\omega \ll \sqrt{2kv_i}$ is given by a generalization of equation (A12) of Laming (2001), which we reproduce here,

$$\gamma = \frac{1}{2} \sqrt{\frac{\pi}{2}} \omega_{pi}^{\prime 2} \left(\frac{\omega}{k v_i}\right)^3 \left(\frac{\omega_{pe}^2 I k_{||}^2 / k^2}{1 + \omega_{pe}^2 / k^2 c^2}\right)^{-1} \left(\vec{k} \cdot \vec{U} - \omega\right) \exp\left[-\left(\omega - \vec{k} \cdot \vec{U}\right)^2 / 2k^2 v_i^2\right], \quad (3)$$

where $I = \frac{m_e}{k_{\rm B}T_e} \int_0^{+\infty} J_0^2 \left(\frac{k_{\perp}v_{\perp}}{\Omega_e}\right) \exp\left(\frac{-m_e v_{\perp}^2}{2T_e}\right) v_{\perp} dv_{\perp}, v_e^2 = k_{\rm B}T_e/m_e, v_i^2 = k_{\rm B}T_i/m_i, J_0\left(\frac{k_{\perp}v_{\perp}}{\Omega_e}\right)$ is the Bessel function of the first kind of order zero and Ω_e is the electron gyrofrequency. The wave frequency in this limit is given by equation (A7) with $\phi = \omega^2/k^2v_i^2 + \dots$

$$\omega^{2} = \frac{\omega_{pe}^{2} \left(k_{\parallel}/k\right)^{2} I / \left(1 + \omega_{pe}^{2}/k^{2}c^{2}\right)}{1 + \omega_{pi}^{2}/k^{2}v_{i}^{2} + (1 - I)\omega_{pe}^{2}/k^{2}v_{e}^{2}}.$$
(4)

The growth rate must exceed the Landau damping rate, γ_{LD} , of the wave due to thermal ions, given by equation (3) with $\vec{k} \cdot \vec{U} = 0$.

Since $\omega \ll \sqrt{2kv_i}$, we may put $\vec{k} \cdot \vec{U} \gg \omega$ and find ω for which $\gamma - \gamma_{LD}$ is maximized. Substituting for k_{\parallel}/k in terms of ω in the expression for $\gamma - \gamma_{LD}$, we find

$$\frac{\partial \left(\gamma - \gamma_{LD}\right)}{\partial \omega} = \gamma \left(\frac{\vec{k} \cdot \vec{U} - 2\omega}{\omega \vec{k} \cdot \vec{U} - \omega^2} - \frac{\omega - \vec{k} \cdot \vec{U}}{k^2 v_i^2}\right) - \gamma_{LD} \left(\frac{2}{\omega} - \frac{\omega}{k^2 v_i^2}\right). \tag{5}$$

Setting this equal to zero we find maxima or minima of ω given by the cubic equation where $\vec{k} \cdot \vec{U} = -kv_s/\alpha$, with v_s the shock velocity and $\alpha = 1/(2\cos\beta)$, where β is the angle between $\partial \omega/\partial \vec{k_\perp}$ and U;

$$\omega^{3} \left[1 + \frac{n'_{i}}{n_{i}} \exp\left(-M^{2}/\alpha^{2}\right) \right] + \omega^{2} \left[\frac{2kv_{s}}{\alpha} \frac{n'_{i}}{n_{i}} \exp\left(-M^{2}/\alpha^{2}\right) \right]$$

$$+ \omega \left[\left(\frac{k^2 v_s^2}{\alpha^2} - 2k^2 v_i^2 \right) \frac{n_i'}{n_i} \exp\left(-M^2/\alpha^2 \right) - 2k^2 v_i^2 \right) \right] - \frac{k v_s}{\alpha} k^2 v_i^2 \frac{n_i'}{n_i} \exp\left(-M^2/\alpha^2 \right) = 0$$
 (6)

where $M = v_s/(\sqrt{2}v_i)$, the Mach number divided by $\sqrt{2}$. For $-kv_s/\alpha >> kv_i$ this has two solutions at $\omega = \sqrt{2}kv_i$ corresponding to minima and a maximum at $\omega = 0$. Looking for more exact solutions near $\omega = 0$ we drop the term in ω^3 and solve the resulting quadratic equation to get

$$\omega = -\alpha \frac{n_i'}{n_i} \sqrt{2kv_i} \frac{(M^2/\alpha^2 + 1)^2}{8M} \exp\left(-M^2/\alpha^2\right). \tag{7}$$

The value of x is then given by

$$x = -\alpha \frac{n_i'}{n_i} \frac{\sqrt{2kv_i} \left(M^2/\alpha^2 + 1\right)^2 \exp\left(-M^2/\alpha^2\right)}{8M\omega_{pe(EM)} \sqrt{I}} \left[1 + \frac{\omega_{pi}^2}{k^2 v_i^2} + \frac{\omega_{pe}^2}{k^2 v_e^2} \left(1 - I\right)\right]^{1/2}$$
(8)

and the growth rate by

$$\gamma - \gamma_{LD} = \sqrt{\frac{\pi}{2}} \frac{n_i'}{n_i} \frac{(M^2/\alpha^2 + 1)^2}{8M} \frac{{\omega_{pi}'}^2 k v_i \exp(-2M^2/\alpha^2)}{k^2 v_i^2 + \omega_{pi}^2 + (1 - I) \omega_{pe}^2 v_i^2 / v_e^2} \left[M - \frac{\alpha^2 (M^2/\alpha^2 + 1)^2}{8M} \right].$$
(9)

It is shown in the Appendix that under a broad range of conditions, $-1 < \alpha < -1/2$. Substituting equation (7) into equation(3) is it easy to see that the growth rate is maximized as $\alpha \to -1$, and that waves grow fastest for the maximum allowable k. In realistic conditions $k_{max} \sim \Omega_e/v_e$, since the electron gyroradius must be shorter than the wavelength for lower hybrid waves. Then for M=1 the growth rate is $\sim 0.04 \left(n_i' \omega_{pi}'^2/n_i \omega_{pe}^2\right) \left(\Omega_e v_e/v_i\right) I/(1-I)$ rad s⁻¹. For M=2 the growth rate is 2 orders of magnitude lower. Thus for $n_i' \sim 0.2n_i$ the growth rates are of order $10^{-2}-10^{-4}\times(v_e/v_i)I/(1-I)$ rad s⁻¹ for plasma parameters similar to those in Figure 8 ($\omega_{pe}=1.8\times10^5$, $\omega_{pi}=3\times10^3$, $\Omega_e=1.8\times10^4$ corresponding to B=1 mG).

The accelerated electron distribution function is given by the generalization of equation (A16) in Laming (2001)

$$f'_{e}\left(v_{||}\right) = \frac{\left(-n'_{i}kv_{s}\exp\left(-M^{2}/\alpha^{2}\right)/\alpha - n_{i}\omega\right)}{\sqrt{2\pi}kv_{i}^{3}} \frac{\omega_{pi}^{2}}{\omega_{pe}^{2}} \left[v_{m} - v_{||} + \frac{\left(v_{m}^{3} - v_{||}^{3}\right)x^{2}}{3v_{Ai}^{2}}\right], \tag{10}$$

where v_m is a constant of integration, the maximum electron velocity where $f'_e(v_m) = 0$. Integrating over $v_{||}$ in the range $0 \to v_m$, and making the approximations $\omega << \sqrt{2}kv_i$, $\vec{k} \cdot \vec{U} = kv_s$ the accelerated electron density is

$$n'_{e} = \frac{n'_{i}}{\sqrt{\pi}v_{i}^{2}} \left[-\frac{M}{\alpha} + \frac{\alpha \left(M^{2}/\alpha^{2} + 1\right)^{2}}{8M} \right] \exp\left(-M^{2}/\alpha^{2}\right) \frac{\omega_{pi}^{2}}{\omega_{pe}^{2}} \left(\frac{v_{m}^{2}}{2} + \frac{v_{m}^{4}x^{2}}{4v_{Ai}^{2}}\right). \tag{11}$$

For reference, the accelerated electron density in the opposite limit, $\omega >> \sqrt{2}kv_i$ is given by (Laming 2001, equation (A17))

$$n'_{e} = \frac{n'_{i}}{\sqrt{2\pi e}v_{i}^{2}} \frac{\omega_{pi}^{2}}{\omega_{pe}^{2}} \left(\frac{v_{m}^{2}}{2} + \frac{v_{m}^{4}x^{2}}{4v_{Ai}^{2}}\right), \tag{12}$$

with $x \simeq \omega_{pi}/\omega_{pe}$. Taking ω to be the lower hybrid frequency, equation (11) is valid for $T_i >> 2.3 \, (B/1 \text{mG})^2 \times 10^9/n_e$ K and equation (12) for $T_i << 2.3 \, (B/1 \text{mG})^2 \times 10^9/n_e$ K. In between these limits Landau damping by thermal ions is sufficiently strong to quench the instability.

To summarize, we have calculated wave dispersion relations and kinetic growth rates in each of the limits $\omega >> \sqrt{2}kv_i$ and $\omega << \sqrt{2}kv_i$. Since these growth rates are in general lower than the ion cyclotron frequency, Ω_i , we also calculate the group velocity of the waves, and by setting this equal to the shock velocity find the angle to the magnetic field at which propagating waves can remain in contact with the shock reflected ions and hence grow to large amplitudes over essentially arbitrary periods of time. For these waves we calculate the growth rates and hence densities of accelerated electrons.

We have revised the velocity range over accelerated electrons may exist from $-v_m \to v_m$ in Laming (2001) to $0 \to v_m$ due to the following consideration. Karney (1978) has derived a value for the maximum electric field above which the wave becomes stochastic and ion heating also commences, given by $E = B \left(\Omega_i/\omega\right)^{1/3} \omega/4/k_{\perp} = B \left(\Omega_i/\omega\right)^{1/3} v_s/2$. The kinetic energy acquired by an electron in time $t \sim 1/\Omega_i$, (the time available for electron acceleration in the precursor before the shock hits) is $(m_i^2/2m_e) \left(E/B\right)^2 x^2/Z^2$, which for relevant values of x and ω evaluates to energies less than 1 keV for Cas A. This is valid for a true perpendicular shock. However it is easy to see that an electron traveling along a magnetic field line inclined at a small angle to the shock front (a quasi-perpendicular shock) can easily stay ahead of the shock and be accelerated to large energies, but may do so traveling in one direction only.

The calculation of the accelerated electron distribution function assumes that the electrons are accelerated purely by Landau damping of the lower hybrid wave, which is likely to be the case for the non-relativistic electrons envisaged here. However since lower hybrid waves exist with $\omega/k_{||} \sim c$, electrons can in principle be accelerated to relativistic energies, if they can be trapped in the wave generation region for long enough. McClements et al. (1997) argue that this is indeed the case for quite a wide range of shock Alfvén Mach numbers, based on the intensity at which lower hybrid waves saturate in simulations and the resulting value of the momentum diffusion coefficient for electrons, and that lower-hybrid waves may provide an electron injection mechanism for subsequent Fermi shock acceleration to cosmic ray energies.

3. Reverse Shock Ionization Structure

3.1. Initial Conditions and Basic Equations

We model the hydrodynamics for the Cas A shell assuming uniform density ejecta and ambient medium. We use expressions given by McKee & Truelove (1995) for the reverse shock radius and velocity with respect to the expanding ejecta, R_r and $\tilde{v_r}$, which connect between the early ejecta dominated, and late Sedov-Taylor limiting behavior. The generalization of such models to non-uniform densities is given in Truelove & McKee (1999). We choose parameters for the hydrodynamic models of Cas A as follows. The blast wave velocity is inferred to be 5200 km s⁻¹ (Vink et al. 1998; Koralesky et al. 1998). The expansion factor $(d \log R_b/d \log t)$ where R_b is the radius of the blast wave) found by these authors to be $\eta = 0.64$ suggests that the remnant is slightly more than midway through the transition between the ejecta dominated and Sedov-Taylor dominated phases, where values of η of 1.0 and 0.4 respectively would be expected. Hence we expect $R_{ST}=2.23\left(M_e/M_\odot\right)^{1/3}n_0^{-1/3}$ pc and $t_{ST}=209E_{51}^{-1/2}\left(M_e/M_\odot\right)^{5/6}n_0^{-1/3}$ years, the transition blast wave radius and time (McKee & Truelove 1995), to be similar to or perhaps slightly smaller than the current values, 2.64 pc and 320 years respectively. In these relations n_0 is the preshock hydrogen density, E_{51} is the explosion energy in units of 10^{51} ergs, and M_e/M_{\odot} is the ejecta mass in units of the solar mass. The ionization age for this shock front is determined to be in the range $10^{11} - 2 \times 10^{11}$ cm⁻³s, (Vink, Kaastra, & Bleeker 1996; Favata et al. 1997), which combined with the age of 320 years gives a preshock electron density of 2.5 - 5.0 cm⁻³, assuming a shock compression of a factor of 4. Taking $R_{ST} = R_b = 2.64$ pc gives M_e/M_{\odot} in the range 4-8. Assuming $t_{ST} = 320$ years gives E_{51} in the range 2.4-4.8. From ASCA observations, Vink, Kaastra, & Bleeker (1996) find $M_e/M_{\odot} \sim 4$. Favata et al. (1997) analyzing BeppoSAX spectra find $2 < M_e/M_{\odot} < 4$, with the uncertainty stemming from different assumptions about the role of the non-thermal continuum. The small ejecta mass is consistent with extensive mass loss as stellar winds by the progenitor. Both references find O to be the dominant element composing the ejecta, with rather little of the expected products of O burning evident, suggesting further that these are confined in a compact stellar remnant. The emission measure quoted by Laming (2001) corresponds to $4M_{\odot}$ of O (if $n_e = 10 \text{ cm}^{-3}$), so in the following we will take $E_{51}=2$, $M_e/M_{\odot}=4$, and $n_0=3$ cm⁻³. This values are similar to those considered by Mochizuki et al. (1999), with the exception of a smaller n_0 . It appears that they chose n_0 consistent with the modeling of Borkowski et al. (1996), who modeled the deceleration of the blast wave upon encountering a shell of circumstellar material postulated to be at the interface of red and blue supergiant presupernova winds, in order to match the measured radio expansion of $\sim 2000 \text{ km s}^{-1}$. The more rapid expansion seen in X-rays (Vink et al. 1998; Koralesky et al. 1998), generally assumed to be more directly associated with the actual motion of the plasma, suggests a lower circumstellar density as used here. Borkowski et al. (1996) do demonstrate in their simulations one important feature relevant in this work, namely the fact that the blast wave (and presumably also the reverse shock) split into transmitted and reflected shocks upon encountering density contrasts, and that these secondary shocks will propagate back across the presumed region of high magnetic field near the contact discontinuity.

The blast wave of Cas A is observed at a radius of 160", while the bright ring of X-ray emission is at a radius of 110" (Vink et al. 1998; Gotthelf et al. 2001). This suggests that the bright ring is in fact emission from the ejecta heated by the reverse shock, since according to the self-similar models of Chevalier (1982), for a blast wave radius of 160", the radius of the contact discontinuity should be in the range 120"-140". Behind the reverse shock, the density n_q of ions with charge q is given by

$$\frac{dn_q}{dt} = n_e \left(C_{ion,q-1} n_{q-1} - C_{ion,q} n_q \right) + n_e \left[\left(C_{rr,q+1} + C_{dr,q+1} \right) n_{q+1} - \left(C_{rr,q} + C_{dr,q} \right) n_q \right] \quad (13)$$

where $C_{ion,q}$, $C_{rr,q}$, $C_{dr,q}$ are the rates for electron impact ionization, radiative recombination and dielectronic recombination respectively, out of the charge state q. These rates are the same as those used in the recent ionization balance calculations of Mazzotta et al. (1998), using subroutines kindly supplied by Dr P. Mazzotta (private communication 2000). The electron density n_e is determined from the condition that the plasma be electrically neutral. The ion and electron temperatures, T_i and T_e are given by generalizations of equation (2) for the case when many charge states of a particular element are present (see Appendix B)

$$\frac{dT_i}{dt} = -0.13n_e \frac{(T_i - T_e)}{AT_e^{3/2}} \frac{\sum_q q^3 n_q / (q+1)}{\sum_q n_q}$$
(14)

and

$$\frac{dT_e}{dt} = 0.13n_e \frac{(T_i - T_e)}{AT_e^{3/2}} \frac{\sum_q q^2 n_q / (q+1)}{\sum_q n_q} - \frac{T_e}{n_e} \left(\frac{dn_e}{dt}\right)_{ion} - \frac{2}{3n_e k_B} \frac{dQ}{dt}.$$
 (15)

Here A is the atomic mass of the ions in the plasma. The last term dQ/dT represents plasma energy losses due to ionization and radiation. Radiation losses are taken from Summers & McWhirter (1978). These authors tabulate the power emitted by each ion of the elements C, O, Si, Ar, Fe and Mo as a function of temperature, allowing an exact treatment of the ionization non-equilibrium aspect of the power losses for these elements. Losses for other elements can be readily obtained by interpolation along isoelectronic sequences. At each time step T_i and T_e are modified by a further factor $\exp(-4v_{ex}/3r)$ and n_e and the n_q by $\exp(-2v_{ex}/r)$, coming from the adiabatic expansion of a spherical shell of plasma with volume $V = 4\pi r^2 dr$ where dr is held constant as r increases. In this approximation, v_{ex} , the expansion velocity, which is constant for all ejecta, is given by the lesser of v_{ex}

 $R_r/t_r - 0.75\tilde{v_r}$ and $v_{ex} = 0.75v_b$, with t_r being the reverse shock onset time, and v_b being the blast wave velocity. This is a reasonable approximation for the transition period between ejecta dominated and Sedov-Taylor evolution in a supernova remnant (see the "hollow" blast wave approximation in Ostriker & McKee 1988). More detailed work could use the self similar solutions appropriate to the various regions and epochs of the remnant evolution (e.g. Chevalier 1982; Hamilton & Sarazin 1984), but even then the inevitable Rayleigh-Taylor instabilities are still difficult to treat. The radius r of the plasma element is given by $r = R_r + \int_{t_0}^t v_{ex} dt$, and we neglect the fact that the rear side of Cas A is around 4pc further away from us than the front side, and thus is observed about 13 years further back in time. Equations (14) and (15) are integrated forwards in time from initial conditions given by the shock jump conditions, equation (1), for the electron and ion temperatures and by the hydrodynamic model discussed above for the densities. All ions are assumed to be singly charged at the time of shock passage, and all ions of the same element are taken to have the same temperature. Our results are insensitive to the exact initial charge state distribution since we are mainly interested in what happens many years after the initial postshock ionization has ceased. In comparisons with the calculations of Mochizuki et al. (1999) for pure Fe ejecta we found agreement to $\pm 10\%$ or better for time dependence of the electron temperature over the lifetime of Cas A.

3.2. Ionization Structure with no Collisionless Electron Heating

Figure 3 shows the evolution of the ion temperature (dashed lines) and the electron temperature (solid lines) for O ejecta heated by reverse shock encounters at various times in the evolution of Cas A. The highest electron temperature, $T_e \simeq 2.7 \times 10^7$ K is found in plasma shocked about 150 years after the supernova. Table 1 gives a summary of the present day values of plasma parameters for different shells of the ejecta shocked at different times after the initial explosion. In Table 2, and illustrated in Figure 4 are similar temperature plots but for circumstellar plasma with elemental composition dominated by N, He and H (in mass ratios 0.02:0.49:0.49 respectively) shocked by the blast wave. Here the highest electron temperature is 7.4×10^7 K, again for plasma shocked 150 years after explosion. This value for the electron temperature is consistent with that actually observed directly behind the blast wave (U. Hwang 2001, private communication), but higher than that observed in spatially integrated spectra. However we believe that the reverse shocked ejecta is the dominant contributor to the observed X-ray emission. Besides the morphological arguments given in the previous section, the blast wave as modeled does not provide enough emission measure to account for the observed emission by a factor of at least 4, remembering that this plasma being composed of less highly charged ions radiates less bremsstrahlung per unit emission measure. Although one could increase the circumstellar density and ejecta mass in the model to match the observations, the explosion energy would also have to be increased as well to to maintain the consistency with the observed blast wave velocity and radius. A problem might still remain however with the likely overproduction of O VIII emission from the dense ejecta cooling at temperatures around 10⁶ K, compared with observations (e.g. Bleeker et al. 2001). Only ejecta which encountered the reverse shock early in the evolution of Cas A (i.e. at times less than 100 years after explosion) has sufficient emission measure to account for the observations.

High values of the ion temperatures in our simulation result simply from the choice of the shock jump conditions, equation (1), as our initial conditions. Some observational support for very high postshock ion temperature exists. Ghavamian et al. (2001) sees broad H α profiles in optical spectra of Tycho, RCW 86 and the Cygnus Loop, commensurate with the shock velocities derived in these remnants. Further, Raymond, Blair, & Long (1995) observing the NW limb of SN 1006 in the UV see broad line profiles for C IV, N V, and O VI, indicating that the heavy ions have similar *velocity* distributions to each other and to the protons, and temperatures proportional to their masses consistent with equation (1).

So we proceed to place the dominant X-ray emission and the electron acceleration in the ejecta. One immediate, but easily solved problem is that according to the ionization balance calculations the temperature of the ejecta shocked at early times should be below 10^6 K, not $\sim 4 \times 10^7$ K as observed. However, if the hard X-rays are due to bremsstrahlung from suprathermal electrons, one should expect just such a temperature deficit in order to be able to accommodate the inevitable Coulomb heating of the ambient plasma due to the accelerated electrons. Cas A emits $\sim 10^{35} {\rm ergs \ s^{-1}}$ above 10 keV. The ratio of radiated bremsstrahlung power to that lost to Coulomb collisions is given approximately by (see e.g. Katz 1987) $Zg\beta^2\alpha_{\rm fs}/(3\sqrt{3}\log\Lambda)$ where $g\sim 1$ is the bremsstrahlung Gaunt factor, $\beta=v/c$, and $\alpha_{\rm fs}$ is the fine structure constant. For Cas A, $Z=8,\ \beta\sim0.2,$ and $\log\Lambda\simeq40$ giving a ratio of $\sim 10^{-5}$. The nonthermal emission above 10 keV thus requires an energy input of $\sim 10^{40} {\rm ergs \ s^{-1}}$, or a total energy input integrated over the lifetime of the remnant of $\sim 10^{50}$ ergs. The electron internal energy in an emission measure of $n_e n_O V = 3 \times 10^{57}$ cm⁻³ for $n_O \sim 2-5 \text{ cm}^{-3}$ (corresponding to ejecta shocked 50 and 100 years after explosion) is $2.5n_eVk_BT \sim 10^{49}$ ergs for a temperature of 4×10^7 K. However the energy required to maintain this quantity of plasma at such temperature against energy losses from ionization, radiation and adiabatic expansion since the initial reverse shock encounter is more than this, $\sim 10^{50}$ ergs, similar in order of magnitude to that available for heating from the accelerated electrons.

3.3. The Inclusion of Accelerated Electrons

To investigate further the effect of the Coulomb heating of the ambient electrons by the accelerated population, we plot in Figure 5 the time dependence of the electron and ion temperatures behind the reverse shock under various heating conditions. We assume a constant heat input per unit volume fixed at the present day value in ejecta reverse shocked about 50 years after the explosion, $\sim 4 \times 10^{-16} \text{ ergs s}^{-1} \text{cm}^{-3}$, (see Appendix B.2 with $n_e = 50$ and $n'_e = 2$). This heating is taken to "switch on" at different times after reverse shock passage. These are taken to be 150, 200, 250, and 300 years. A physical mechanism for such a "switch on" is suggested by the morphology of SN 1987A. The blast wave must encounter a strong density gradient before reflected shocks can travel back towards the contact discontinuity. Thus a certain amount of time may elapse while the blast waves reaches this density gradient and the reflected shock propagates back. In SN 1987A the relevant density gradient would be provided by the inner edge of the presumed equatorial disk, the recombination radiation from which currently produces the inner ring. In Cas A no real evidence for such an equatorial disk exists, but shock reflection from a distribution of quasistationary flocculi is the main possibility. From Figure 5 it is apparent that electron heating beginning 200-250 years after reverse shock passage (or after 250-300 years in the evolution of the supernova remnant, i.e. between curves d and e) will reproduce the current observed electron temperature of $\sim 4 \times 10^7$ K. Figure 1 illustrates this with spectra from the BeppoSAX MECS (Boella et al. 1997) and PDS (Frontera et al. 1997) instruments acquired on 1997 November 26, plotted against a pure thermal bremsstrahlung spectrum at 4×10^7 K and a similar spectrum including an extra 4% of electrons in an accelerated distribution function. Also shown are seven data points from a rocket flight on 1968 December 5 (Gorenstein, Kellogg, & Gursky 1970). These are shown in more detail in Figure 6 plotted against pure thermal bremsstrahlung spectra corresponding to temperatures of 2×10^7 , 3×10^7 and 4×10^7 K. From Figure 5 it is clear that on the basis of the hydrodynamic models used in these calculations, the ambient electron temperature should have increased between these two observations by $\sim 2 \times 10^7$ K. Depending on how one treats line emission and interstellar absorption (both omitted from the theoretical spectra in Figure 5), such a temperature increase is marginally consistent with the observations. The ionization age $n_e t$ in such a case would be $\sim 10^{11} \ \mathrm{cm^{-3} s^{-1}}$, a factor of ~ 2 lower than observations (Vink, Kaastra, & Bleeker 1996; Favata et al. 1997). Curves b and c in Figure 5, representing electron acceleration starting 150 or 200 years after explosion (100 or 150 years after reverse shock passage) give values of $n_e t$ more consistent with observations, but temperatures in the range 5-6 keV. The heating mechanism envisaged here only occurs at perpendicular shocks, and so not all the ejecta will be heated. Consequently a thermal conduction energy loss from the heated regions might be expected, which would reduce the peak temperature and reduce the degree of temperature increase that might be expected between the observations of Gorenstein, Kellogg, & Gursky (1970) and the present day. One interesting feature of curves b and c is that the initial period of heating from 10^4 K to $\sim 2 \times 10^5$ K is very fast, but then slows abrubptly. The "plateau" at this temperature is due to the strong peak in the O radiative loss curve at this temperature, and the plasma temperature only starts to rise again once it has expanded sufficiently to reduce the density so that the collisionless heating can overcome the strong radiative losses.

We will now investigate in more detail exactly where in the Cas A ejecta a two stream instability that provides lower hybrid wave electron heating may occur. In the picture that we develop, the X-ray emitting shell of Cas A is filled with shocks propagating in all directions as a result of forward or reverse shock interactions with density inhomogeneities. In the hot ion limit, where $\omega \ll \sqrt{2kv_i}$ the wave growth rates fall dramatically with increasing Mach number, so we can reasonably assume that only shocks with the minimum Mach number to be supercritical are important. For plasma β (ratio of gas pressure to magnetic pressure) of 1 this Mach number is 1.7 for perpendicular shocks, falling to 1.35 for $\beta = 2$ (Edmiston & Kennel 1984). A further simplifying assumption will be to assume that the accelerated electrons heat the ambient plasma to the observed temperature, 4×10^7 K, and then that the instability continues in marginal stability. This is a lesser criterion on the electron energization process than the ambient electron heating discussed above. In such conditions, the values of the parameters I and $(k_{\perp}/2) \partial I/\partial k_{\perp}$ in equation (A7) are ~ 0.5 and ~ -0.25 respectively. The accelerated electron density is maximized for a given k at $-M/\alpha \simeq 0.7$ from equation (11). This is a lower value than is realizeable in practice, the minimum value being $-M/\alpha \simeq 1$ for high β plasmas and short wavelength waves. At marginal stability, the electron plasma β_e is given by $\beta_e = 8\pi n_e k T_e/B^2 = 2\omega_{pe}^2 v_e^2/\Omega_e^2/c^2 = 2$. In heavy element plasma with highly charged ions the electrons dominte the total plasma β , so $M \simeq 1$. For $k = \omega_{pe}/c = \Omega_e/v_e$, $-\alpha = 0.5 - 0.6$ (from Figure 7), so $-M/\alpha \simeq 2$. Decreasing β , allowing larger k and hence larger (i.e. more negative) α also requires larger M, so $-M/\alpha \simeq 2$ holds over the range of reasonable values of β , k, and α . Assuming $n'_i/n_i = 0.2$ for the shock reflected ions, which is comparable to that observed in situ at solar wind shocks (e.g. Gedalin 1996), the fraction of electrons accelerated is given by $n'_e/n_e = 0.05/v_i^2$ where $v_m = 1.5 \times 10^{10}$ cm s⁻¹ has been used in equation (11). This corresponds to 70 atomic units found as the best match to BeppoSAX data in Laming (2001).

The density of accelerated electrons may be increased over that given by equation (11) if the energetic electrons are pitch angle scattered away from the magnetic field direction. This scattering mainly results from collisions with ions, while energy loss is due to collisions with ambient electrons. The isotropic density of accelerated electrons, $n'_{e,iso}$ is given by $n'_{e,iso} \sim n'_e \tau_{e,e}/\tau_{e,i} \sim 4n'_e$. The electron-electron and electron-ion scattering cross sections

have the same dependence on the energy of the accelerated electron, and so the isotropic accelerated electrons will have the same energy distribution as those directed along the magnetic field. This pitch angle scattering boosts the accelerated electron density by a factor ~ 5 for the same reflected ion density. Hence an accelerated electron fraction of 4% may be possible in regions of the Cas A ejecta where $v_i < 2.5 \times 10^7$, i.e. $T_i < 6 \times 10^7$ K.

¿From Table 2 we see that ejecta reverse shocked up to ~ 100 years after the initial explosion may support sufficient electron acceleration to account for the observations. In this context it is important to realize, however, that ejecta shocked within 100 years of the explosion can have a low enough ion temperature to justify using equation (12) for the accelerated electron density, which would increase the accelerated electron fraction by around an order of magnitude over that given by equation (11). In general cool plasma instabilities are stronger than those in hot plasma, and so our conclusion that electrons can be accelerated in ejecta shocked early in the evolution of Cas A will be strengthened.

Hence our model for the electron acceleration to form the hard X-ray tail by non-thermal bremsstrahlung and to provide heating of the ambient ejecta plasma to $\sim 4 \times 10^7$ K by Coulomb collisions requires the existence of shocked ejecta that has cooled to give ion temperatures well below $\sim 10^8$ K. This requires that secondary shocks passing through this ejecta have velocities below ~ 500 km s⁻¹ so as to avoid reheating the ions up to temperatures where the instability weakens. This is actually quite likely, since a shock reflected for example from the blast wave moving through the shocked circumstellar medium will slow down considerably upon reaching the shell ejecta shell.

4. Discussion

We have previously argued (Laming 1998, 2000, 2001) that two stream instabilities formed ahead of fast shock fronts in supernova remnants might more realistically be modeled as kinetic rather than reactive instabilities. This is observationally motivated, in that the degree of electron heating predicted by models based on reactive instabilities (e.g Cargill & Papadopoulos 1988) is not observed (Laming et al. 1996; Ghavamian et al. 2001). A theoretical justification comes from the fact that high Mach number shocks are turbulent and not steady state structures, and reflected ions consequently will not form a "beam", but will inhabit a much wider portion of phase space, giving rise to kinetic instabilities. With their lower growth rates, these will generally allow insufficient wave growth ahead of the shock before being overrun by the shock itself. In this paper we have avoided this problem by focusing on lower hybrid waves formed ahead of the shock that have group velocity away from the shock equal to the shock velocity itself, and hence stay in contact with the shock

reflected ions for sufficiently long times to allow significant wave growth to occur.

In this paper we have found that the most efficient electron acceleration occurs for the lowest Mach number shocks, just above the first critical Mach number, which is where shock is said to become "supercritical". This denotes the onset of turbulence in the shock structure, and ion reflection which becomes progressively more unsteady and "bursty" in nature as the Mach number increases (e.g. Tokar et al. 1986). Hence although we considered the lower hybrid instability excited by the secondary shocks in the Cas A shell to be kinetic in nature since this appears to be a more robust assumption, the results of our calculations suggest that in this case reactive instabilities could be quite plausible also. It is also worth remarking that the designation "reactive" or "kinetic" comes from the mathematical treatment of two different limits of the Vlasov equation (see Appendix A), and that physically, a continuum of instabilities exists between the kinetic and reactive limits. The further investigation of these would require numerical simulations. All instabilities in this paper have a minimum wavector $k_{min} \sim \omega_{pe}/c$ arising from electromagnetic effects and a maximum $k_{max} \sim \Omega_e/v_e$ from the requirement that the electron gyroradius be smaller than the wavelength. In marginal stability $k_{min} \sim k_{max}$ allowing us to estimate the magnetic field stength, $B = m_e v_e \omega_{pe}/e = 5.9 \omega_{pe} \times 10^{-9}$, which evaluates to 1.9 mG for $\omega_{pe} = 4 \times 10^5$ rad s⁻¹ in the t=50 year ejecta. From Table 1 the ejecta shocked at 50 years after explosion occupies a volume $\sim 2 \times 10^{55}$ cm⁻³, in order to give the stated emission measure. The magnetic energy contained in this volume is 3×10^{48} ergs, not inconsistent with that deduced from the minimum energy synchrotron luminosity argument (Longair 1994).

These magnetic fields are assumed to be amplified from seed fields by the action of a Rayleigh-Taylor instability (though see Lou 1994, for another possibility). Plausible evidence of this has recently been demonstrated in imaging spectroscopy of Cas A by Chandra (Hughes et al. 2000; Hwang, Holt, & Petre 2000). In the SE quadrant of Cas A in particular, emission in Fe L and K shell lines is observed to be *outside* the emission from the lighter element Si, suggesting that the Si burning zone in the progenitor (which produced the Fe) has overtaken the O burning zone which produced the Si. This region in the SE is also where recent XMM-Newton observations find the hardest continuum (Bleeker et al. 2001), though these authors comment that the hard X-ray continuum emission actually is distributed quite uniformly over the remnant, which argues in favor of an emission mechanism independent of the magnetic field, i.e. bremsstrahlung, and not e.g. synchrotron emission. We have previously argued that the secondary shocks that excite the lower hybrid waves arise as the blast wave encounters density inhomogeneities in the circumstellar medium producing reflected shocks as in Borkowski et al. (1996). However another possibility exists which is perhaps more intimately associated with Fe emission and Rayleigh-Taylor instability, viz. the reverse shock encountering Fe-Co-Ni bubbles in the ejecta (Li, McCray, & Sunyaev 1993; Borkowski et al. 2000). The simulation in the last reference demonstrates that such a scenario would produce large amounts of turbulence and vigorous mixing of Fe with the overlying ejecta. We also note in passing that the idea of secondary shocks propagating through already shocked material, and also being highly magnetic, has been successfully applied to ultraviolet spectra of the bowshock in HH 47A by Hartigan et al. (1999). In this case the strong magnetic field arises as radiatively cooling gas is compressed by hotter material around it. This is also possible but in our view unlikely for the regions of Cas A we discuss.

A common parameter quoted in models for electron heating is the fraction of the shock energy that is deposited in the electrons. It is not possible to make such a statement about the secondary shocks responsible for the electron acceleration in our model of Cas A, but in terms of the blast wave energy an estimate can be made. If the 10^{40} ergs s⁻¹ required to accelerate the electrons comes from secondary shocks that originate from the blast wave, this energy is to be compared with the energy $\sim 4\pi R_b^2 v_s n_i k_B T_i \simeq 10^{41}$ ergs s⁻¹ deposited by the blast wave in the shocked ions. Neglecting energy going into cosmic ray ions, around 10% of the blast wave energy ends up in energized electrons to be compared with the $\sim 20\%$ estimated by (e.g. Cargill & Papadopoulos 1988).

The electron distribution function is given by balancing the imaginary terms in the dielectric response, which give wave growth due to shock reflected ions and Landau damping by the accelerated electrons. We argue that secondary shocks maintain this electron distribution against the inevitable losses due to Coloumb collisions, and that therefore these shocks must pass through a plasma element on timescales significantly shorter than those for Coloumb collisions, which are of order 2 - 40 years for accelerated electrons of energy 10 - 70 keV in the ejecta shocked at early times. The accelerated electron distribution will be different from that modeled above if processes other than electron Landau damping occur. McClements et al. (1997) argue that sufficient lower hybrid wave intensity is likely to exist such that electrons may be accelerated by a stochastic mechanism to mildly relativistic energies, but that this is more easily satisfied at high Alfvén Mach number shocks.

5. Conclusions

In Laming (2001) it was shown that in principle a distribution of electrons accelerated by lower hybrid waves comprising about 4% of the plasma electrons produced a very good match to existing spectra of Cas A from BeppoSAX. This model used cold plasma theory, assuming $\omega >> \sqrt{2}kv_i$. In this paper we have extended the plasma theory to treat the opposite limit $\omega << \sqrt{2}kv_i$, and by performing calculations of the time dependent ionization balance within

the ejecta of Cas A, have identified regions where such wave generation may take place.

In ejecta shocked ~ 150 years or more since explosion, only the thermal plasma instability ($\omega << \sqrt{2}kv_i$) may occur. However this instability appears to be too weak to provide significant electron heating to give the hard X-ray emission. In ejecta shocked up to ~ 100 years since the explosion, either the cold or thermal plasma instabilities ($\omega >> \sqrt{2}kv_i$) can occur, depending on the ion temperature. The cold plasma instability is more likely, and is sufficiently strong to explain the putative hard X-ray bremsstrahlung. Such electron heating and acceleration mechanisms may plausibly occur elsewhere, the main requirement being a sufficently strong magnetic field. We have concentrated our efforts on Cas A since it has the most conspicuous hard X-ray emission, is well studied in other respects, and is thought to have undergone relatively little elemental mixing (Johnston & Yahil 1984) which renders the plasma theory more tractable.

This work was supported by basic research funds of the Office of Naval Research and has also made use of data obtained from the High Energy Astrophysics Science Archive Research Center (HEASARC) provided by NASA's Goddard Space Flight Center.

A. Appendix: Lower Hybrid Waves

A.1. Reactive and Kinetic Instabilities

In cold plasma, the dispersion relation for lower hybrid waves, omitting the electromagnetic terms is given by (e.g. Vaisberg et al. 1983; McClements et al. 1997; Laming 2001)

$$K^{L} = 1 + \frac{\omega_{pe}^{2}}{\Omega_{e}^{2}} \sin^{2}\theta - \frac{\omega_{pi}^{2}}{\omega^{2}} - \frac{\omega_{pe}^{2}}{\omega^{2}} \cos^{2}\theta = 0$$
(A1)

where ω is the wave frequency, ω_{pe} and Ω_{e} are the electron plasma frequency and gyrofrequency respectively, ω_{pi} is the ion plasma frequency and θ is the angle between the direction of wave propagation and the magnetic field vector. As $\sin \theta \to 1$ this gives $\omega \to \Omega_{LH}$ where $\Omega_{LH} = \sqrt{\Omega_{e}\Omega_{i}}$, the geometric mean of the electron and ion gyrofrequencies, known as the lower hybrid frequency. In the presence of suprathermal ions the dispersion relation is modified by the addition of the following term to the expression for K^{L} ;

$$+\frac{\omega'^2}{n_i'k^2} \int \frac{\vec{k} \cdot \vec{v_i}}{\omega} \frac{\vec{k}}{\omega - \vec{k} \cdot \vec{v_i}} \cdot \frac{\partial f_i'}{\partial \vec{v_i}} d^3 \vec{v_i}$$
 (A2)

where ω'_{pi} $f'(v_i)$ and n' are the plasma frequency, distribution function and density of the suprathermal ions with velocity v_i , and \vec{k} is the wavevector with magnitude k.

If $\partial f'/\partial v_i = 0$ at $\omega = \vec{k} \cdot \vec{v_i}$ then the integral may be evaluated in a straightforward manner. Taking the most extreme limit in this case we put $f' = n'\delta\left(\vec{v_i} - \vec{v_b}\right)$ for a monoenergetic ion beam moving with velocity $\vec{v_b}$, and the integral evaluates to $\omega_{pi}^2/\left(w - \vec{k} \cdot \vec{v_b}\right)^2$. With the addition of this term to the expression for K^L the dispersion relation becomes a quartic equation analogous to that for the Buneman instability, the complex roots of which (when present) give growing or damping waves. Physically the wave growth is driven by the free energy in the ion beam as a whole. Such instabilities are known as "reactive" instabilities and usually give very fast growth rates.

In the opposite limit we make the replacement $\omega \to \omega + i\gamma$ assuming $\gamma << \omega$ and evaluate the integral by going into the complex plane. This procedure is summarized by the so-called Landau prescription

$$1/\left(\omega - \vec{k} \cdot \vec{v_i}\right) \to P\left(1/\left(\omega - \vec{k} \cdot \vec{v_i}\right)\right) - i\pi\delta\left(\omega - \vec{k} \cdot \vec{v_i}\right). \tag{A3}$$

Upon making this replacement, taking imaginary parts and rearranging, an equation for the growth rate γ in terms of the integral $\int \left(\vec{k}\cdot\partial f'/\partial\vec{v_i}\right)\delta^3\left(\omega-\vec{k}\cdot\vec{v_i}\right)d^3\vec{v_i}$ results (see Laming 2001, for the full expression). In this limit the instability is called "kinetic", and is physically due to stimulated Cerenkov emission of plasma waves. For wave growth, $\partial f'/\partial v_i > 0$, or in other words a population inversion must exist. This makes the analogy with quantum physics clear, and indeed one can discuss the various wave-wave and wave-particle interactions in terms of the appropriate Feynman diagrams.

Reactive and kinetic instabilities derive from the different mathematical treatments of the term in the dispersion relation accounting for the suprathermal ions. Of course in reality a continuum of instabilities exists between these two limits, but further investigation of these requires numerical techniques.

A.2. The Dispersion Relation in Thermal Plasma

In finite temperature plasma, the general expression for the longitudinal part of the dielectric tensor is (Melrose 1986)

$$\begin{split} K^{L} = & 1 + \frac{4\pi q^{2}}{\omega^{2}} \int \sum_{s=-\infty}^{+\infty} \frac{1}{\omega - s\Omega_{e} - k_{||}v_{||}} \frac{\left(s\Omega_{e} + k_{||}v_{||}\right)^{2}}{k^{2}} J_{s}^{2} \left(\frac{k_{\perp}v_{\perp}}{\Omega_{e}}\right) \left(\frac{\omega - k_{||}v_{||}}{v_{\perp}} \frac{\partial}{\partial p_{\perp}} + k_{||} \frac{\partial}{\partial p_{||}}\right) f\left(\vec{p}\right) d^{3}\vec{p} \\ = & 1 - \frac{\omega_{pe}^{2}}{\omega^{2}} \frac{\omega m_{e}}{k^{2}k_{\mathrm{B}}T_{e}} \sum_{s=-\infty}^{+\infty} \int_{-\infty}^{+\infty} \frac{s^{2}\Omega_{e}^{2} + k_{||}^{2}v_{||}^{2} + 2s\Omega_{e}k_{||}v_{||}}{\omega - s\Omega_{e} - k_{||}v_{||}} \left(\frac{m_{e}}{2\pi k_{\mathrm{B}}T_{e}}\right)^{3/2} \exp\left(-m_{e}v_{||}^{2}/2k_{\mathrm{B}}T_{e}\right) d\psi_{||} A4) \\ & \times \int_{0}^{+\infty} J_{s}^{2} \left(\frac{k_{\perp}v_{\perp}}{\Omega_{e}}\right) \exp\left(-m_{e}v_{\perp}^{2}/2k_{\mathrm{B}}T_{e}\right) 2\pi v_{\perp} dv_{\perp}. \end{split}$$

Here ω is the wave frequency, $k_{||}$ and k_{\perp} are the components of the wavevector k parallel and perpendicular to the magnetic field B direction. Ω_e is the electron cyclotron frequency, v and p are the electron velocity and momentum, with subscripts having the same meaning as for the wavevector, and J_s is the Bessel function of the first kind of order s. Assuming $k_{||}v_{||} << \omega - s\Omega_e$ in denominator, appropriate for lower-hybrid waves, the expression simplifies to

$$K^{L} = 1 - \frac{\omega_{pe}^{2}}{\omega^{2}} \frac{1}{k^{2}} \sum_{s=-\infty}^{+\infty} \frac{\omega}{\omega - s\Omega_{e}} \left[s^{2} \Omega_{e}^{2} \left(\frac{m_{e}}{k_{B} T_{e}} \right)^{2} + k_{\parallel}^{2} \left(\frac{m_{e}}{k_{B} T_{e}} \right) \right]$$

$$\times \int_{0}^{+\infty} J_{s}^{2} \left(\frac{k_{\perp} v_{\perp}}{\Omega_{e}} \right) \exp\left(-m_{e} v_{\perp}^{2} / 2k_{B} T_{e} \right) 2\pi v_{\perp} dv_{\perp}.$$
(A5)

The term in s = 0 is

$$K_{s=0}^{L} = -\frac{\omega_{pe}^{2} k_{||}^{2}}{\omega^{2} k^{2} k_{\mathrm{B}} T_{e}} \int_{0}^{+\infty} J_{0}^{2} \left(\frac{k_{\perp} v_{\perp}}{\Omega_{e}}\right) \exp\left(-m_{e} v_{\perp}^{2} / 2k_{\mathrm{B}} T_{e}\right) 2\pi v_{\perp} dv_{\perp}, \tag{A6}$$

while the terms in $s \neq 0$ are evaluated by converting the $\sum_{-\infty}^{+\infty} \to \sum_{1}^{+\infty}$. Using the standard property of the Bessel functions, $1 - J_0^2(z) = 2 \sum_{s=1}^{\infty} J_s^2(z)$, and assuming $\omega \ll 0$ gives

$$K_{|s|>0}^{L} = \frac{\omega_{pe}^{2}}{k^{2}} \left(\frac{m_{e}}{k_{B}T_{e}}\right)^{2} \int_{0}^{+\infty} \left[1 - J_{0}^{2} \left(\frac{k_{\perp}v_{\perp}}{\Omega_{e}}\right)\right] \exp\left(-m_{e}v_{\perp}^{2}/2k_{B}T_{e}\right) 2\pi v_{\perp} dv_{\perp}. \tag{A7}$$

Including the term for thermal ions, $\omega_{pi}^2/k^2v_i^2\left(1-\phi\left(\frac{\omega}{\sqrt{2}kv_i}\right)\right)$, where the usual plasma dispersion function is $\phi(z)=-z/\sqrt{\pi}\int_{-\infty}^{\infty}\exp\left(-t^2\right)/\left(t-z\right)dt$, a term unity for the vacuum, and inserting an electromagnetic correction, $\omega_{pe}^2\to\omega_{pe}^2/\left(1+\omega_{pe}^2/k^2c^2\right)$, for the electron term involving $k_{||}$ (Begelman & Chiueh 1988; Melrose 1986) the dispersion relation is

$$\omega^{2} = \frac{\omega_{pe}^{2} \left(I k_{||}^{2} / k^{2} \right) / \left(1 + \omega_{pe}^{2} / c^{2} k^{2} \right)}{1 + \frac{\omega_{pi}^{2}}{k^{2} v_{e}^{2}} \left(1 - \phi \right) + \frac{\omega_{pe}^{2}}{k^{2} v_{e}^{2}} \left(1 - I \right)}$$
(A8)

where $I = \frac{m_e}{k_{\rm B}T_e} \int_0^{+\infty} J_0^2 \left(\frac{k_{\perp}v_{\perp}}{\Omega_e}\right) \exp\left(\frac{-m_e v_{\perp}^2}{2T}\right) v_{\perp} dv_{\perp}, v_e^2 = k_{\rm B}T_e/m_e \text{ and } v_i^2 = k_{\rm B}T_i/m_i.$

A.3. Group Velocities

Proceeding as in the cold plasma case, we differentiate equation (A8) with respect to k_{\perp} to derive an expression for the group velocity;

$$\begin{split} \frac{\partial \omega}{\partial k_{\perp}} &= \frac{-\omega}{k} \frac{k_{\perp}}{k} + \frac{\omega \omega_{pe(EM)}^2}{k^3 c^2} \frac{k_{\perp}}{k} + \frac{\omega}{2I} \frac{\partial I}{\partial k_{\perp}} \\ &+ \frac{\omega}{2} \left[\frac{2\omega_{pi}^2}{k^3 v_i^2} \frac{k_{\perp}}{k} \left(1 - \phi \right) + \frac{\omega_{pi}^2}{k^2 v_i^2} \frac{\partial \phi}{\partial k_{\perp}} + \frac{2\omega_{pe}^2}{k^3 v_e^2} \frac{k_{\perp}}{k} \left(1 - I \right) + \frac{\omega_{pe}^2}{k^2 v_e^2} \frac{\partial I}{\partial k_{\perp}} \right] \left[1 + \frac{\omega_{pi}^2}{k^2 v_i^2} \left(1 - \phi \right) + \frac{\omega_{pe}^2}{k^2 v_e^2} \left(1 - I \right) \right] (A9) \end{split}$$

where $\omega_{pe(EM)}^2 = \omega_{pe}^2 / (1 + \omega_{pe}^2 / c^2 k^2)$.

In the limit $\omega >> \sqrt{2}kv_i$, $\phi \to 1 + k^2v_i^2/\omega^2 + 3k^4v_i^2/\omega^4 + \dots$ We set $\partial \omega/\partial k_\perp = v_s = \alpha\omega/k_\perp$ where v_s is the shock velocity and $\alpha = 1/\left(2\cos\beta\right)$ where β is the angle between $\partial \omega/\partial \vec{k}_\perp$ and \vec{U} , the bulk velocity of the shock reflected ion distribution. With $x = k_{||}/k$ to lowest order in $\omega_{pi}^2/\omega_{pe}^2$,

$$x^{4} \left[-\frac{\omega_{pe(EM)}^{4}I}{k^{2}c^{2}} + \frac{\omega_{pe(EM)}^{2}I}{1+\omega_{pe}^{2}(1-I)/k^{2}v_{e}^{2}} \right] +$$

$$x^{2} \left[\omega_{pe(EM)}^{2} \frac{k_{\perp}}{2} \frac{\partial I}{\partial k_{\perp}} - \alpha \omega_{pe(EM)}^{2}I + \frac{\omega_{pe(EM)}^{4}I}{k^{2}c^{2}} + \frac{\left(\omega_{pe(EM)}^{4}I/k^{2}v_{e}^{2}\right)(k_{\perp}/2)\partial I/\partial k_{\perp} - \omega_{pe(EM)}^{2}I}{1+\omega_{pe}^{2}(1-I)/k^{2}v_{e}^{2}} \right] +$$

$$+\omega_{pi}^{2} - \alpha \omega_{pi}^{2} + \frac{\left(\omega_{pi}^{2}\omega_{pe}^{2}/k^{2}v_{e}^{2}\right)(k_{\perp}/2)\partial I/\partial k_{\perp}}{1+\omega_{pe}^{2}(1-I)/k^{2}v_{e}^{2}} = 0.$$
(A10)

This looks like a quadratic equation in x^2 , but we must remember that $k^2 = k_\perp^2/(1-x^2)$, $\omega_{pe(EM)} \to \omega_{pe}$ and rewrite in terms of k_\perp , which gives a quartic equation for x^2 . However we are looking for solutions $x^2 << 1$, for which both quartic and quadratic equations give the same result to leading order in $\omega_{pi}^2/\omega_{pe(EM)}^2$. For $x^2 << 1$, in the limit $k_\perp v_e/\Omega_e \to 0$, where $I \simeq 1 - k_\perp^2 v_e^2/\Omega_e^2$ and $(k_\perp/2) \, \partial I/\partial k_\perp \simeq I - 1$ this has solution

$$x^{2} \simeq \frac{\alpha}{-\alpha - 1 + \omega_{pe(EM)}^{2}/k^{2}c^{2}} \left(\omega_{pi}^{2}/\omega_{pe(EM)}^{2}\right). \tag{A11}$$

In the cold plasma approximation, $\omega_{pe(EM)}^2/k^2c^2 \to 0$ and $x^2 = \omega_{pi}^2/\omega_{pe}^2$ for $\alpha = -1/2$ (i.e. reflected ions returning to the shock). This is the result given previously (McClements et al. 1997; Laming 2001). The electromagnetic correction however has the effect of forcing the minimum wavevector to be $k = \omega_{pe}/c$. We require $x^2 > 0$ which gives $k^2 > -\alpha\omega_{pe}^2/c^2/(\alpha+1)$. As $k_{\perp}v_e/\Omega_e$ increases from 0 the minimum wavevector decreases and reflected ions leaving the shock can excite the necessary waves. For $k_{\perp}v_e/\Omega_e \sim 1$, so that $I \simeq 0.5$ and $(k_{\perp}/2) \partial I/\partial k_{\perp} \simeq -0.25$ with $\omega_{pe} >> kv_e$

$$x^{2} = \frac{1 - 2\alpha}{1 + \alpha - \omega_{pe(EM)}^{2}/k^{2}c^{2}} > 0$$
 (A12)

which requires $\omega_{pe(EM)}^2/k^2c^2 - 1 < \alpha < 1/2$. Figure 7 shows x^2 against $k_{\perp}v_e/\Omega_e$ for $\alpha = 1/2$ and $k^2 = \omega_{pe}^2/c^2$ (bold curve), taking $\omega_{pe} = 4 \times 10^5$, $\omega_{pi} = 7 \times 10^3$, and $\omega = 560$ corresponding to $n_e = 50$ and $n_i = 6.25$ cm⁻³ and a magnetic field of 1.9 mG. The other curves show the loci of x^2 for k^2 multiplied by factors of 1/2, 2, and 4 (as labeled) from this value. Apart from the fact that it is now ions leaving the shock that excite the waves, the value of x^2 is still essentially the same as that found in the cold plasma case, i.e. $x^2 \sim \omega_{pi}^2/\omega_{pe}^2$.

Now if $k \sim \omega_{pe}/c$, the approximation $\omega >> \sqrt{2}kv_i$ may be no longer valid in regions of Cas A, and we investigate the opposite limit of the plasma dispersion function, $\omega << \sqrt{2}kv_i$.

In between these two limits, where $\omega \sim \sqrt{2kv_i}$ Landau damping by thermal ions will prevent any wave growth. In the opposite limit $\phi \to \omega^2/k^2v_i^2 + \dots$ and

$$x^{2} = 1 - \frac{\alpha \left[1 + \omega_{pi}^{2}/k^{2}v_{i}^{2} + (1 - I)\omega_{pe}^{2}/k^{2}v_{e}^{2} \right] - (k_{\perp}/2I)\partial I/\partial k_{\perp} \left(1 + \omega_{pi}^{2}/k^{2}v_{i}^{2} + \omega_{pe}^{2}/k^{2}v_{e}^{2} \right)}{\left[1 + \omega_{pi}^{2}/k^{2}v_{i}^{2} + (1 - I)\omega_{pe}^{2}/k^{2}v_{e}^{2} \right]\omega_{pe(EM)}^{2}/k^{2}c^{2} - 1},$$
(A13)

which can be rearranged to give

$$\alpha = (1 - x^{2}) \left[\frac{\omega_{pe}^{2}}{k^{2}c^{2} + \omega_{pe}^{2}} - \frac{1}{1 + \omega_{pi}^{2}/k^{2}v_{i}^{2} + (1 - I)\omega_{pe}^{2}/k^{2}v_{e}^{2}} + \frac{k_{\perp}}{2I} \frac{\partial I}{\partial k_{\perp}} \frac{1 + \omega_{pi}^{2}/k^{2}v_{i}^{2} + \omega_{pe}^{2}/k^{2}v_{e}^{2}}{1 + \omega_{pi}^{2}/k^{2}v_{i}^{2} + (1 - I)\omega_{pe}^{2}/k^{2}v_{e}^{2}} \right].$$
(A14)

Again in the limit of low electron temperatures for $x^2 \ll 1$

$$\alpha = \frac{\omega_{pe}^2}{k^2 c^2 + \omega_{pe}^2} - \frac{1 + \omega_{pi}^2 v_e^2 / \Omega_e^2 v_i^2 + \omega_{pe}^2 / \Omega^2}{1 + \omega_{pe}^2 / \Omega_e^2 + \omega_{pi}^2 / k^2 v_i^2}.$$
 (A15)

For $\omega_{pe}^2 >> \Omega_e^2$ this reduces to $\alpha = \frac{\omega_{pe}^2}{k^2c^2+\omega_{pe}^2} - 1$ and satisfies $\alpha < -1/2$ for $k > \omega_{pe}/c$. In the opposite limit of high electron temperature, $I \to 0$, $k_\perp \partial I/\partial k_\perp \to -I$, and $\alpha = -1/\left(1+\omega_{pi}^2/k^2v_i^2\right)$ giving the more usual value $k_{min} = \omega_{pi}/v_i$ (see Laming 2001). However in this limit the lower hybrid waves do not exist, and so the appropriate wavevector for lower hybrid wave growth is $k = \omega_{pe}/c$, arising from the electromagnetic correction. In Figure 7 we show the generalization of this result to arbitrary electron temperature. The loci of α for $x^2 = 0$ are plotted against $k_\perp v_e/\Omega_e$, taking the following plasma parameters for Cas A, $\omega_{pe} = 1.8 \times 10^5$, $\omega_{pi} = 3 \times 10^3$, and $\omega = 300$, corresponding to $n_e = 10$ and $n_i = 1.25$ cm⁻³, and a magnetic field of 1 mG. The bold curve shows the value of α for $k = \omega_{pe}/c$, while the curves show α ($k_\perp v_e/\Omega_e$) for values of k successively factors of 2 greater. The dotted line shows $\alpha = -1/2$, remembering that necessarily $\alpha < -1/2$ for ions reflected back through the upstream plasma with relative velocity approximately twice the shock velocity. In this limit wave propagating at a variety of small cosines, x to the magnetic field vector can stay in contact with shock reflected ions. The wave direction that dominates will be that where the net growth rate is maximized, as determined in section 2.

B. Appendix: Collision Processes

B.1. Electron-Ion Coulomb Equilibration

Spitzer (1978) gives the timescale for an electron distribution to relax to a Maxwellian

$$t_{eq}(e,e) = \frac{3m_e^{1/2} (k_{\rm B}T_e)^{3/2}}{4\pi^{1/2} n_e e^4 \ln \Lambda}$$
 (B1)

where Λ is the so-called plasma parameter, the ratio of largest to smallest impact parameters for collisions. In supernova remnants $\ln \Lambda \simeq 40$. The equilibration time for ions $t_{eq}(i,i) = t_{eq}(e,e) \sqrt{m_i/m_e}/Z_i^4$, and that for electron-ion equilibration is $t_{eq}(e,i) = t_{eq}(e,e) m_i/m_e/Z_i^2$ where Z_i is the ion charge. Accordingly we write

$$\frac{d\Delta T}{dt} = -0.13Z^2 n_e \frac{\Delta T}{AT_e^{3/2}} \tag{B2}$$

which is equation (2), with $\Delta T = T_i - T_e$. We consider a fully ionized gas with $n_e = Zn_i$ and

$$\frac{d}{dt}(n_iT_i + n_eT_e) = n_i\frac{dT_i}{dt} + n_e\frac{dT_e}{dt} = 0.$$
 (B3)

Solving these equations yields

$$\frac{dT_e}{dt} = 0.13 \frac{Z^2 n_e}{Z+1} \frac{T_i - T_e}{AT_e^{3/2}}$$
 (B4)

$$\frac{dT_i}{dt} = -0.13 \frac{Z^3 n_e}{Z+1} \frac{T_i - T_e}{A T_e^{3/2}}.$$
 (B5)

In deriving equations (14) and (15) these expressions are averaged over the ion charge states in the plasma, and the expression for dT_e/dt is modified by the inclusion of terms accounting for the change in electron density due to ionization, $-(T_e/n_e)(dn_e/dt)_{ion}$, and radiative and ionization losses, $-(2/3n_ek_B)dQ/dt$. Recombinations, which reduce the electron density do not result in an increase in the electron temperature in low density plasmas, since the energy of the recombined electron is radiated away, rather than being shared with the other plasma electrons as would be the case for three-body recombination in dense plasmas.

B.2. Collisional Relaxation of Accelerated Electron Distribution

The Boltzmann equation for the electron distribution function f is (see e.g. Sturrock 1994)

$$\frac{\partial f}{\partial t} = -\Gamma \frac{\partial}{\partial v_r} \left(f \frac{\partial H}{\partial v_r} \right) + \frac{\Gamma}{2} \frac{\partial^2}{\partial v_r \partial v_s} \left(f \frac{\partial^2 G}{\partial v_r \partial v_s} \right)$$
 (B6)

where $G = \int f |\vec{v} - \vec{v_1}| d^3 \vec{v_1}$ and $H = 2 \int f / |\vec{v} - \vec{v_1}| d^3 \vec{v_1}$ are the Rosenbluth potentials and $\Gamma = (4\pi e^4/m_e^2) \log (3\pi\Lambda)$ where Λ is the usual plasma parameter. For the collisional relaxation of a suprathermal electron distribution f with a background Maxwellian f_1 the Rosenbluth potentials take the forms

$$\frac{\partial^2 G}{\partial v_r \partial v_s} = \int f_1(v_1) \left[\frac{\delta_{rs}}{|\vec{v} - \vec{v_1}|} - \frac{(v_s - v_{s1})(v_r - v_{r1})}{|\vec{v} - \vec{v_1}|^3} \right] d^3 \vec{v_1}$$
(B7)

$$\frac{\partial H}{\partial v_r} = 2n_e \left[-\frac{v_r}{v^3} \Phi\left(\beta v\right) + \frac{1}{v} \frac{\partial \Phi(\beta v)}{\partial v} \right]$$
 (B8)

where $\Phi(\beta v) = 2/\sqrt{\pi} \int_0^{\beta v} \exp(-x^2) dx$ with $\beta^2 = m_e/2k_BT_e$. For a suprathermal electron distribution with $v_{||} >> 1/\beta$, $\Phi(\beta v) = 1$. Working in one dimension then $\partial^2 G/\partial v_{||}^2 = 0$ and $\partial H/\partial v_{||} = -2n_e/v_{||}^2$. Hence

$$\frac{\partial f}{\partial t} = 2\Gamma n_e \frac{\partial}{\partial v_{||}} \left(\frac{f}{v_{||}^2} \right) \tag{B9}$$

with $f\left(v_{||}\right) = n_e' \left[v_m - v_{||} + \left(v_m^3 - v_{||}^3\right)x^2/3v_{\mathrm{A}i}^2\right]/\left(v_m^2/2 + v_m^4x^2/4v_{\mathrm{A}i}^2\right)$, where v_m is the maximum electron velocity in the distribution, $v_{\mathrm{A}i}$ is the Alfvén speed and x is the cosine of the angle between the magnetic field vector and \vec{k} . In the cold plasma limit $\cos\theta = \omega_{pi}/\omega_{pe}$ so $v_{\mathrm{A}i}/x$ may be identified with the electron Alfvén speed. The energy loss rate of the suprathermal electron distribution, which is equal in magnitude (but opposite in sign) to the heating rate of the ambient electrons, is given by

$$\int \frac{1}{2} m_e v_{||}^2 \frac{\partial f}{\partial t} dv_{||} = -\frac{\Gamma n_e n_e' m_e}{v_m^2 / 2 + v_m^4 x^2 / 4 v_{Ai}^2} \left[2 \left(v_m + \frac{v_m^3 x^2}{3 v_{Ai}^2} \right) \log \frac{v_m}{v_{th}} - v_m + \frac{v_m^3 x^2}{9 v_{Ai}^2} \right].$$
(B10)

Taking the lower limit of integration to be $v_{th} = 6 \times 10^9$ cm s⁻¹, corresponding to an electron energy of 10 keV, where the ambient and accelerated electron densities are approximately equal, $v_m \simeq 2.5 v_{th} \simeq 1.5 \times 10^{10}$ cm s⁻¹, and equation (B5) evaluates to an energy input from accelerated electrons to the ambient plasma of $4 \times 10^{-18} n_e n'_e$ ergs cm⁻³s⁻¹ for $v_{Ai} \sim x v_m$.

REFERENCES

Aharonian, F. et al. 2001, A&A, 370, 112

Allen, G. E., et al. 1997, ApJ, 487, L97

Begelman, M. C., & Chiueh, T. 1988, ApJ, 332, 872

Bingham, R., Dawson, J. M., Shapiro, V. D., Mendis, D. A., & Kellett, B. J. 1997, Science, 275, 49

Bingham, R. Kellett, B. J., Dawson, J. M., Shapiro, V. D., & Mendis, D. A. 2000, ApJS, 127, 233

Bleeker, J. A. M., Willingale, R., van der Heyden, K., Dennerl, K., Kaastra, J. S., Aschenbach, B., & Vink, J. 2001, A&A, 365, L225

Boella, G., et al. 1997, A&AS, 122, 327

Borkowski, K. J., Szymkowiak, A. E., Blondin, J. M., & Sarazin, C. L. 1996, ApJ, 466, 866

Borkowski, K. J., Blondin, J. M., Lyerly, W. J., & Reynolds, S. P. 2000, in Cosmic Explosions, 10th Maryland Astrophysics Conference, eds. S. S. Holt & W. W. Zhang, 173

Burrows, D. N., Michael, E., Hwang, U., McCray, R., Chevalier, R. A., Petre, R., Garmire, G., Holt, S. S., & Nousek, J. A. 2000, ApJ, 543, L149

Bykov, A. M., & Uvarov, Yu. A. 1999, JETP, 88, 465

Cargill, P. J., & Papadopoulos, K. 1988, ApJ, 329, L29

Chevalier, R. A. 1982, ApJ, 258, 790

Dieckmann, M. E., McClements, K. G., Chapman, S. C., Dendy, R. O., & Drury, L. O'C. 2000, A&A, 356, 377

Edmiston, J. P., & Kennel, C. F. 1984, J. Plasma Phys., 32, 429

Favata, F., Vink, J., Dal Fiume, D., Parmar, A. N., Santangelo, A., Mineo, T., Preite-Martinez, A., Kaastra, J. S., & Bleeker, J. A. M. 1997, A&A, 324, L49

Fransson, C., Lundqvist, P., & Chevalier, R. A. 1996, ApJ, 461, 993

Frontera, F., et al. 1997, A&AS, 122, 357

Gedalin, M. 1996, J. Geophys. Res., 101, 4871

Ghavamian, P. Raymond, J. C., Smith, R. C., & Hartigan, P. 2001, ApJ, 547, 995

Gorenstein, P., Kellogg, E. M., & Gursky, H. 1970, ApJ, 160, 199

Gotthelf, E. V., Koralesky, B., Rudnick, L., Jones, T. W., Hwang, U., & Petre, R. 2001, ApJ, 552, L39

Gringauz, K. I., et al. 1986, Nature, 321, 282

Hamilton, A. J. S., & Sarazin, C. L. 1984, ApJ, 281, 682

Hartigan, P., Morse, J. A., Tumlinson, J., Raymond, J. C., & Heathcote, S. 1999, ApJ, 512, 901

Hughes, J. P., Rakowski, C. E., Burrows, D. N., & Slane, P. O. 2000, ApJ, 528, L109

Hughes, J. P., Rakowski, C. E., & Decourchelle, A. 2000, ApJ, 543, L61

Hwang, U., Holt, S. S., & Petre, R. 2000, ApJ, 537, L119

Johnston, M. D., & Yahil, A. 1984, ApJ, 285, 587

Karney, C. F. F. 1978, Phys. Fluids, 21, 1584

Katz, J. I. 1987, High Energy Astrophysics, (Menlo Park, CA: Addison Wesley Publishing Company Inc.)

Klimov, S. S., et al. 1986, Nature, 321, 292

Koralesky, B., Rudnick, L., Gotthelf, E. V., & Keohane, J. V. 1998, ApJ, 505, L27

Koyama, K., Petre, R., Gotthelf, E. V., Hwang, U., Matsuura, M., Ozaki, M., & Holt, S. S. 1995, Nature, 378, 255

Koyama, K., Kinugasa, K., Matsuzaki, K., Nishiuchi, M., Sugizaki, M., Torii, K., Yamauchi, S., & Aschenbach, B. 1997, PASJ, 49, L7

Krasnosel'skikh, V. V., Kruchina, E. N., Thejappa, G., & Volokitin, A. S. 1985, A&A, 149, 323

Laming, J. M., Raymond, J. C., McLaughlin, B. M., & Blair, W. P. 1996, ApJ, 472, 267

Laming, J. M. 1998, ApJ, 499, 309

Laming, J. M. 2000, ApJS, 127, 409

Laming, J. M. 2001, ApJ, 546, 1149

Li, H., McCray, R., & Sunyaev, R. A. 1993, ApJ, 419, 824

Longair, M. S. 1994, High Energy Astrophysics, Vol. 2, Stars, the Galaxy and the Interstellar Medium (Cambridge: Cambridge University Press)

Lou, Y.-Q. 1994, ApJ, 428, L21

Mazzotta, P., Mazzitelli, G., Colafrancesco, S., & Vittorio, N. 1998, A&AS, 133, 403

McClements, K. G., Dendy, R. O., Bingham, R., Kirk, J. G., & Drury, L. O'C. 1997, MNRAS, 291, 241

McKee, C. F., & Truelove, J. K. 1995, Physics Reports, 256, 157

Melrose, D. B. 1986, Instabilities in Space and Laboratory Plasmas, (Cambridge: Cambridge University Press)

- Mochizuki, Y., Takahashi, K., Janka, H.-Th., Hillebrandt, W., & Diehl, R. 1999, A&A, 346, 831
- Ostriker, J. P., & McKee, C. F. 1988, Rev. Mod. Phys., 60, 1
- Raymond, J. C., Blair, W. P., & Long, K. S. 1995, ApJ, 454, L31
- Reber, G. 1944, ApJ, 100, 279
- Ryle, M., & Smith, F. G. 1948, Nature, 162, 462
- Shapiro, V. D., Bingham, R., Dawson, J. M., Dobe, Z., Kellett, B. J., & Mendis, D. A. 1999, J. Geophys. Res., 104, 2537
- Shimada, N., & Hoshino, M. 2000, ApJ, 543, L67
- Slane, P., Gaensler, B. M., Dame, T. M., Hughes, J. P., Plucinsky, P. P., & Green, A. 1999, ApJ, 525, 357
- Slane, P., Hughes, J. P., Edgar, R. J., Plucinsky, P. P., Miyata, E., Tsunemi, H., & Aschenbach, B. 2001, ApJ, 548, 814
- Spitzer, L. Jr., Physical Processes in the Interstellar Medium, (New York: Wiley)
- Sturrock, P. A. 1994, Plasma Physics, (Cambridge: Cambridge University Press)
- Summers, H. P., & McWhirter, R. P. 1978, J. Phys. B., 12, 2387
- Tidman, D. A., & Krall, N. A. 1971, Shock Waves in Collisionless Plasmas, (New York: Wiley-Interscience)
- Tokar, R. L., Aldrich, C. H., Forslund, D. W., & Quest, K. B. 1986, Phys. Rev. Lett., 56, 1059
- Truelove, J. K., & McKee, C. F. 1999, ApJS, 120, 299, erratum ApJS, 128, 403
- Vaisberg, D. L., Galeev, A. A., Zastenker, G. N., Klimov, S. I., Nozdrachev, M. N., Sagdeev, R. Z., Sokolov, A. Y., & Shapiro, V. D. 1983, Sov. Phys. JETP, 58, 716
- Vink, J., Kaastra, J. S., & Bleeker, J. A. M. 1996, A&A, 307, L41
- Vink, J., Bloemen, H., Kaastra, J. S., & Bleeker, J. A. M. 1998, A&A, 339, 201

- Fig. 1.— Data from the BeppoSAX MECS and PDS instruments with model bremsstrahlung spectra for a fully ionized oxygen plasma. The softest model spectrum is pure thermal bremsstrahlung. The harder spectrum has an additional 4% of electrons accelerated by lower hybrid waves to a maximum velocity of $v_m = 1.5 \times 10^{10}$ cm s⁻¹ (see eq. 10). The seven data points in bold print are taken from a rocket observation in 1968 (Gorenstein, Kellogg, & Gursky 1970) to illustrate the stability of at least the thermal part on the spectrum.
- Fig. 2.— Cartoon of the Cas A supernova remnant (not to scale) showing the location of the blast wave or forward shock, the reverse shock and the contact discontinuity between the reverse shocked ejecta and the forward shocked circumstellar medium. Also shown schematically are a few quasi-stationary flocculi (QSFs) ahead of the forward shock and fast moving knots of ejecta (FMKs) ahead of the reverse shock. As the forward and reverse shocks encounter these density contrasts, they split into transmitted and reflected shocks. The reflected shocks can propagate back across the contact discontinuity. Cas A has numerous knots and clumps of material, making it likely that the entire shell is filled with these secondary shocks.
- Fig. 3.— The variation of ion temperature (dashed lines) and electron temperature (solid lines) for reverse shocks in Cas A in pure oxygen ejecta, against time since explosion. The evolution of the temperatures is plotted for ejecta encountering the reverse shock at various times (50, 60, 75, 100, 150, 200, and 250 years after the initial explosion), and followed to 350 years after the explosion. The present day corresponds to t=321 years, for an explosion date of 1680. The most dense ejecta is that which encounters the reverse shock earliest, and in this calculation undergoes radiative instability at around 120 years after explosion.
- Fig. 4.— Similar to Figure 1 but for forward shocks in Cas A at 50, 150, and 250 years since explosion. The elemental composition is now a mixture of N/He/H, (in mass ratios 0.02:0.49:0.49) corresponding to that observed in the quasi-stationary flocculi. The electron temperature is again the solid line, the N ion temperatures are the dashed lines, He ion temperatures the dotted lines, and the proton temperatures the dash-dot lines. Very little ion-ion or electron-ion equilibration has occurred.
- Fig. 5.— Variation of ion (dashed lines) and electron temperature (solid lines) in pure oxygen ejecta reverse shocked at 50 years after the initial explosion, with electron reheating by lower hybrid waves commencing a further 100, 150, 200, and 250 years since reverse shock passage, represented by the curves labeled "b", "c", "d", and "e" respectively. Curve "a" shows the initial heating and cooling following reverse shock passage, and is the same as in

This preprint was prepared with the AAS LATEX macros v5.0.

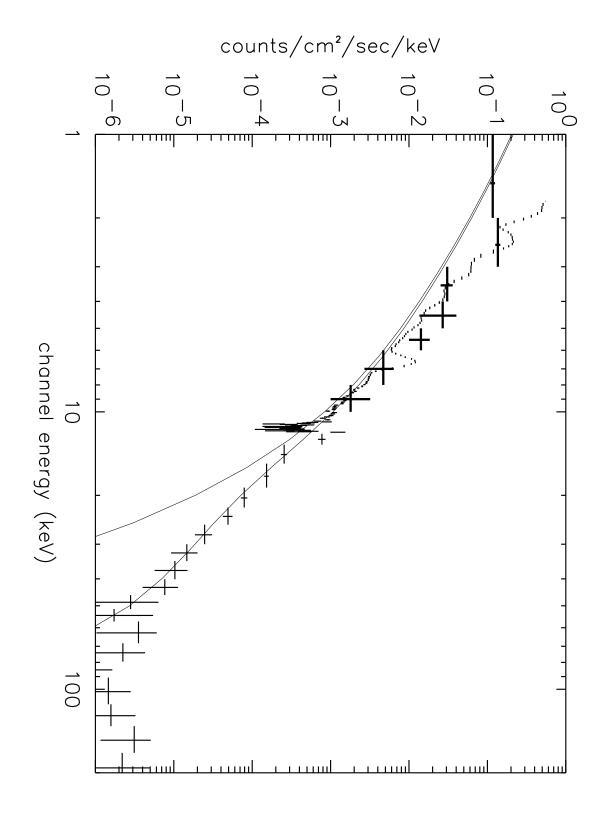
- Figure 3. The electron temperature is assumed to go no lower than 10^4 K, being maintained at this level by residual photoionization and conduction. The electron heating is taken to be the same as the present day value, per unit volume. The presently observed electron temperature is $\sim 4 \times 10^7$ K, which is consistent with the curve with reheating commencing between 250-300 years since explosion, or 200-250 years since reverse shock passage.
- Fig. 6.— Data points from (Gorenstein, Kellogg, & Gursky 1970) plotted against pure thermal bremsstrahlung spectra corresponding to temperatures of 2×10^7 , 3×10^7 , and 4×10^7 K.
- Fig. 7.— The variation of direction cosine squared, $x^2 = k_{\parallel}^2/k^2$ against $k_{\perp}v_e/\Omega_e$ for $\alpha = 1/2$ taking $\omega_{pe} = 4 \times 10^5$, $\omega_{pi} = 7 \times 10^3$, and $\omega = 560$ corresponding to $n_e = 50$ and $n_i = 6.25$ cm⁻³ and a magnetic field of 1.9 mG. The bold curve gives the loci of x^2 for $k^2 = \omega_{pe}^2/c^2$. The other curves gives loci for k^2 equal to 1/2, 2, and 4 times this value, as labeled. For $k_{\perp}v_e/\Omega_e \leq 1$ direction cosines less than ω_{pi}/ω_{pe} are found, in accordance with the cold plasma treament.
- Fig. 8.— The variation of α with $k_{\perp}v_e/\Omega_e$ for various values of k_{\perp} . The plasma parameters taken are $\omega_{pe}=1.8\times10^5$, $\omega_{pi}=3\times10^3$, and $\omega=300$, corresponding to $n_e=10$ and $n_i=1.25$ cm⁻³, and a magnetic field of 1 mG. The top curve gives $k_{\perp}=\omega_{pe}/c$. The successively lower curves are for $k_{\perp}=a\omega_{pe}/c$ where a=1.778, 3.162, 10, and 100 respectively.

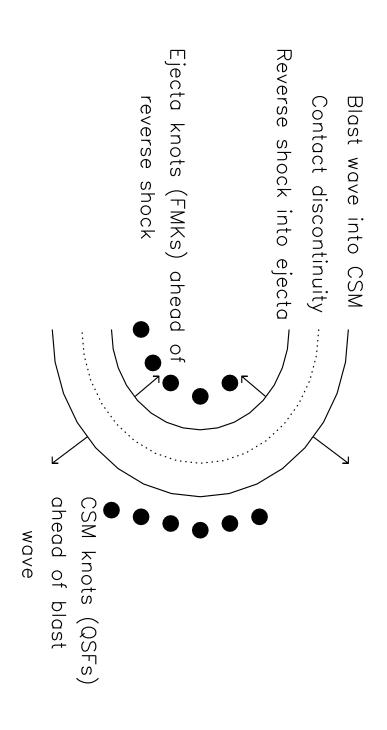
Table 1. Reverse Shock Parameters from Ionization Structure

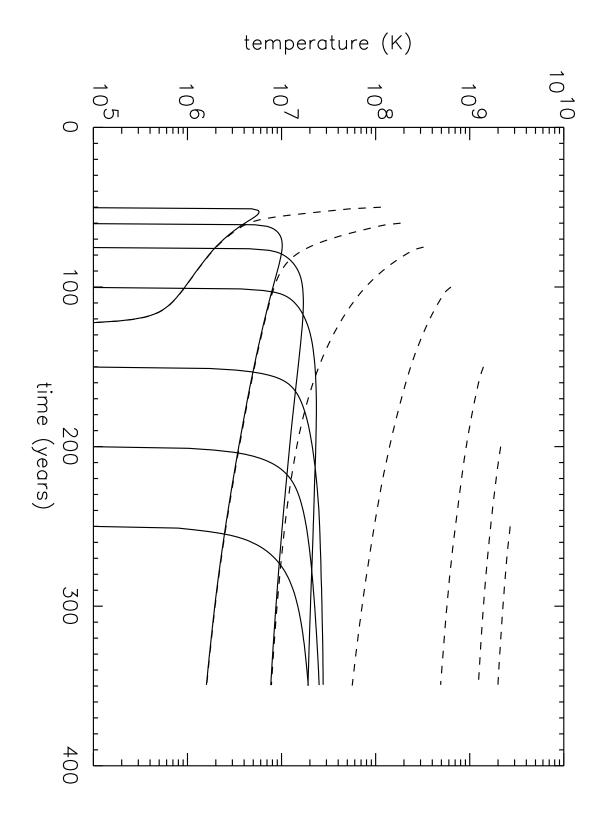
t (years)	q	T_i (K)	T_e (K)	$n_e (\mathrm{cm}^{-3})$	$n_e t \text{ (cm}^{-3} \text{s)}$	approx. EM (cm^{-3})
50	0.726	1.00e4	1.00e4	51.8		5e57
100	0.551	6.48e7	1.98e7	23.0	2.33e11	8e56
150	0.432	5.36e8	2.73e7	11.8	6.89e10	3e56
200	0.348	1.32e9	2.37e7	6.75	2.20e10	1e56
250	0.286	2.13e9	1.71e7	3.83	6.51e9	6e55
300	0.240	2.87e9	6.05e6	2.00	7.35e8	3e55

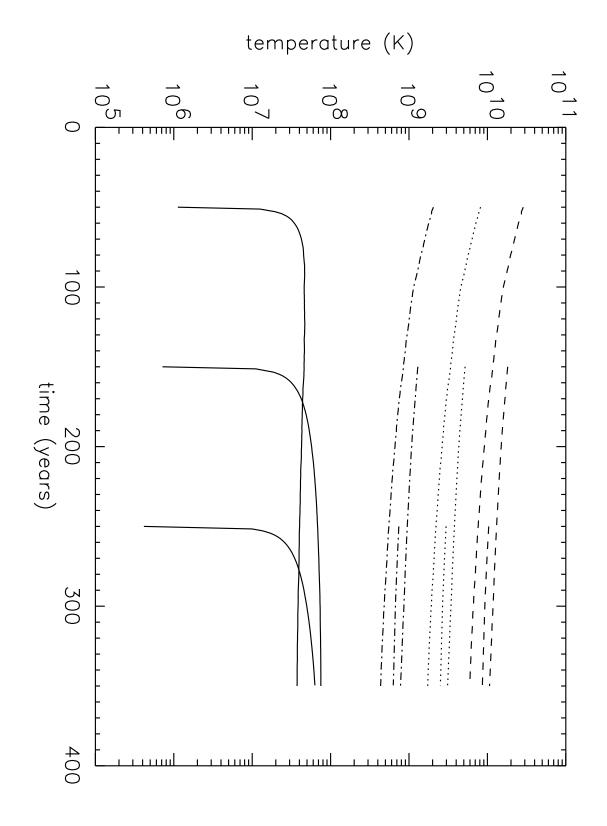
Table 2. Forward Shock Parameters from Ionization Structure

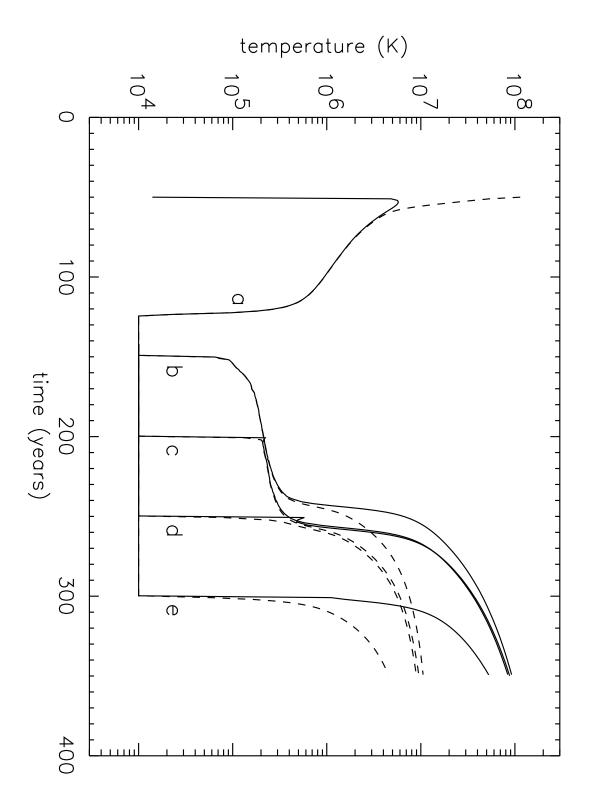
t (years)	T_N (K)	T_{He} (K)	T_H (K)	T_e (K)	$n_e (\mathrm{cm}^{-3})$	$n_e t \text{ (cm}^{-3}\text{s)}$	approx. EM (cm^{-3})
50	6.30e9	1.83e9	4.59e8	3.70e7	0.96	1.58e10	2e55
100	1.02e10	2.98e9	7.48e8	6.48e7	2.73	2.33e10	2e56
150	1.13e10	3.30e9	8.27e8	7.45e7	4.58	2.32e10	5e56
200	1.05e10	3.06e9	7.67e8	7.02e7	6.20	1.93e10	1e57
250	8.99e9	2.61e9	6.53e8	5.63e7	7.44	1.27e10	1.5e57
300	7.46e9	2.14e9	5.37e8	3.12e7	8.56	4.17e9	2e57

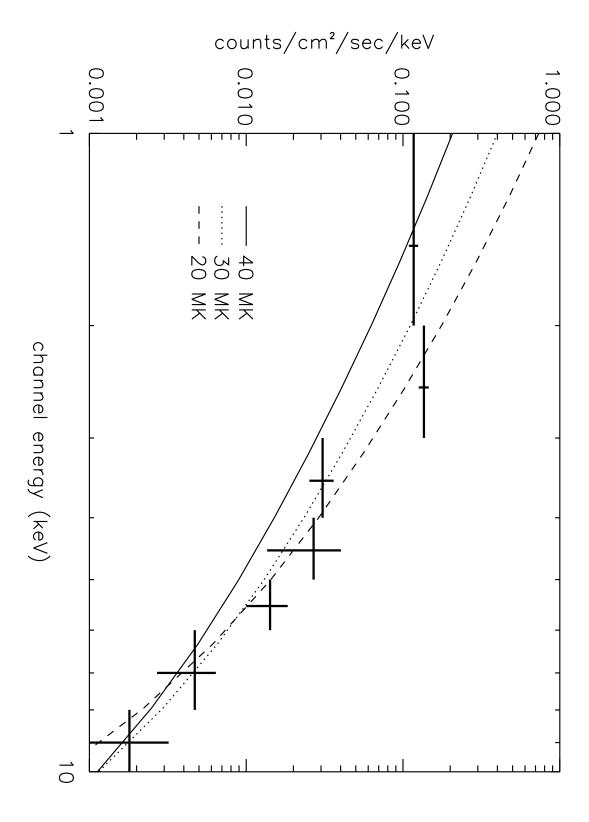












 k_{\parallel}^{2}/k^{2} in units $\omega_{pi}^{2}/\omega_{pe}^{2}$

